Structural transformation and photoluminescence modification of $AgInS_2$ nanoparticles induced by ZnS shell formation

Yasushi Hamanaka[1]*, Daichi Yukitoki[1], and Toshihiro Kuzuya[2]

[1]*Department of Materials Science and Engineering, Nagoya Institute of Technology, Nagoya 466-8555, Japan*

[2]*College of Design and Manufacturing Technology, Muroran Institute of Technology, Muroran 050-8585, Japan*

E-mail: hamanaka@nitech.ac.jp

$AgInS_2$ nanoparticles were capped by ZnS via a widely used procedure to fabricate core/shell nanoparticles with highly efficient luminescence. The nanoparticle structures were investigated by ultrahigh-resolution analytical electron microscopy. We found that Zn–Ag–In–S nanoparticles were created by ZnS capping at ~480 K, which suggests that the luminescence enhancement reported for such core/shell nanoparticles is not because of the passivation of surface defects by ZnS shells, but Zn-doping. Quasi-core/shell nanoparticles could be obtained by ZnS capping without heating. However, their luminescence efficiency remained unchanged, indicating that surface passivation was ineffective when ZnS shells were formed at room temperature.

During the last three decades, colloidal semiconductor nanoparticles (NPs) have attracted considerable interest because of remarkable progress in wet chemical synthetic methods enabling the large-scale, low-cost production of highly luminescent NPs.[1), 2)] Among them, type II–VI NPs such as CdSe have been most actively studied as typical examples of semiconductor quantum dots that exhibit various size-dependent optical properties originating from the quantum confinement effect of carriers.[3), 4)] More strong and stable luminescence can be achieved by fabricating core/shell structures in which the CdSe core is capped by a thin layer of semiconductors with larger bandgaps.[5), 6)] ZnS is typically selected for the shell material because it can passivate existing defects on surfaces of CdSe NPs acting as the nonradiative recombination centers. Recently, the same procedure has been applied to ternary chalcopyrite NPs with type I–III–VI_2 compositions (e.g., $AgInS_2$ (AIS), $CuInS_2$ (CIS), etc.), which are promising fluorescent NPs as more eco-friendly because of their less toxic (Cd-free) compositions. Many studies have reported that AIS and CIS NPs capped by ZnS shells exhibit improved luminescence with quantum yields (QYs) of up to ~0.8.[7)-11)] Simultaneously, capping with ZnS leads to a slight blue shift in the luminescence bands.[8)-10)] However, similar high-efficiency luminescence together with the blue shift has been observed in Zn-doped I–III–VI_2 NPs with quaternary compositions (e.g., Zn–Ag–In–S NPs).[12)-15)] These results suggest that the significant enhancements in luminescence efficiencies observed in I–III–VI_2 NPs after ZnS capping are possibly because of the doping of Zn ions into the NP bodies, rather than surface passivation. However, actual core/shell structures have not yet been identified in chalcopyrite NPs. Therefore, the precise analysis of a single chalcopyrite NP is required to conduct a thorough investigation of the mechanisms of luminescence enhancement induced by ZnS capping.

In this paper, we report the characteristic morphologies of individual AIS NPs modified by ZnS shells determined by ultrahigh-resolution analytical microscopy along with the corresponding luminescence analyses. Our results indicate that the ZnS capping procedure typically used for chalcopyrite NPs allows Zn atoms to easily penetrate into the AIS NPs, resulting in conversion to the quaternary NPs.

AIS NPs with an average diameter of 2.6 nm were synthesized via solution-phase reactions between Ag–In thiolate and S-dodecanethiol complexes.[16)] ZnS shells were formed around the AIS NPs using two methods. The first is an analogue of the standard method used for synthesizing CIS/ZnS and AIS/ZnS core/shell NPs, which has been already reported by many researchers.[7)-11)] In this method, AIS NPs were mixed with zinc octanoate,

sulfur powder, and dodecanethiol in octadecene, followed by the addition of oleylamine. The mixtures were heated to 483 K and kept for an hour under a flow of inert gas. The second is a nonheating method; AIS NPs dispersed in hexane were mixed with zinc acetate followed by the addition of oleylamine. A sulfur/dodecanethiol solution was then injected dropwise under an inert gas atmosphere and stirred continuously for three days at room temperature. When the reactions were complete, both NPs were washed with ethanol and centrifuged to remove excess precursors and ligands before analyses. In this paper, the two NPs capped with ZnS at 483 K and at room temperature are abbreviated as "w/-heating" and "w/o-heating" NPs, respectively.

Figures 1 and 2 show the high-angle annular dark-field scanning transmission electron microscopy (HAADF-STEM) images of the w/o-heating and w/-heating NPs taken on a JEM-ARM200F scanning transmission electron microscope and the elemental mapping images of the corresponding areas obtained using energy dispersive X-ray spectroscopy (EDS). In the HAADF-STEM image of the w/o-heating NPs (Fig. 1(a)), spherical particles of diameter ~3 nm, comparable to the original AIS NPs, surrounded by nanostructured products with irregular shapes are observed. The elemental images (Fig. 1(b)-(f)) show that Ag and In are primarily distributed inside of the NPs, Zn is distributed in the surrounding areas, and S is detected in both locations. Such characteristic morphologies indicate that the room-temperature ZnS-capping procedure provides quasi-core/shell NPs comprising AIS cores and ZnS shells. However, this method results in incomplete capping because the shell thickness is inhomogeneous (some parts are very thin), and the NP shapes are irregular, implying a noncrystalline nature. Conversely, such composite structures are not observed in the w/-heating NPs (Figure 2(a)). The elemental mapping images show that Ag, In, Zn, and S are uniformly distributed in individual NPs (Fig. 2(b)-(f)). This indicates that Zn atoms are easily introduced into AIS NPs to form quaternary NPs when heated (~480 K) during the capping process. The average diameter of the individual w/-heating NPs is 3–5 nm, which is relatively large as compared to the original AIS NPs. To the best of our knowledge, the capping of I–III–VI_2 NPs with ZnS that produced drastic enhancements in luminescence has typically been conducted at 470–500 K.[7)-11)] Our result strongly suggests that luminescence enhancement due to alloying in such NPs cannot be ruled out.

To obtain deeper insights into the detailed structures of NPs after the ZnS capping treatments, we recorded X-ray diffraction (XRD) patterns. Figure 3 shows that the XRD pattern of the original AIS NPs matches well with the standard pattern of tetragonal AIS. As in many other reports,[8)-10)] the main diffraction peaks shift toward higher angles and

approach the peak positions of cubic ZnS after ZnS capping treatments both with and without heating. These results indicate the formation of core/shell structures or alloying; however, further structural analysis is impossible because of the broadening of the diffraction peaks caused by the small sizes of the NPs. Thus, instead of XRD, we have employed spectroscopic analyses to obtain new insights into the structures of individual NPs.

The absorption and photoluminescence (PL) spectra of the original AIS, w/-heating NPs, and w/o-heating NPs are shown in Fig. 4. Shoulder absorption peaks are observed around 2.6 eV in the spectra of both AIS and w/o-heating NPs. The energy positions of these peaks are higher than the bandgap energy of bulk AIS, 1.87 eV;[17] therefore, these peaks are attributed to the transition between the lowest quantized levels in the valence and conduction bands due to the quantum confinement effect of carriers. An additional strong peak at 4.4 eV was observed for the w/o-heating NPs, which might originate from the ZnS shells.[18] The similar spectral shapes below ~3.5 eV in the spectra of the original and w/o-heating NPs indicate that sizes and compositions of the AIS cores remain unchanged when ZnS shell is formed without heating. The shoulder absorption peak at around 2.6 eV was also observed in the spectrum of the w/-heating NPs. This energy is equivalent to that observed for the original AIS NPs, indicating that the bandgap energy is comparable to that of the AIS NPs despite the quaternary compositions of the w/-heating NPs. Bandgap widening that is dependent on Zn content has been reported for Zn–Ag–In–S alloyed NPs.[12)-15)] Therefore, the comparable bandgap energy is attributed to relatively weak quantum confinement because of the larger sizes of the w/-heating NPs.

The PL peak energies for the original AIS, w/o-heating NPs, and w/-heating NPs are 1.69, 1.76, and 1.88 eV, respectively. The PL spectra show large Stokes shifts of 0.7–0.9 eV from the shoulder absorption peaks, which is typical of the PL features of I–III–VI_2 NPs due to defect-related emission. The ZnS capping treatments with and without heating result in the blue-shifting of the PL bands, although the absorption peak energies remain unchanged. Such blueshifts have often been reported for I–III–VI_2 NPs after alloying or doping with Zn.[12)-15)] Therefore, some amounts of Zn ions are introduced into the AIS cores of the w/o-heating NPs as well as in the w/-heating NPs with quaternary compositions. The PL peak shifts may be due to the creation of point defects related to Zn ions, which form a novel intragap level that acts as a new recombination path.

The PL-QYs of the original AIS, w/o-heating NPs, and w/-heating NPs were estimated to be 0.242 ± 0.014, 0.191 ± 0.009, and 0.081 ± 0.004, respectively. Numerous studies

have reported that the PL-QYs of AIS and CIS NPs increase after capping with ZnS. However, in this study, the PL-QY decreased slightly even in the w/o-heating NPs with quasi-core/shell structures. This result suggests the incomplete passivation of the surface defects in the AIS cores, which is supported by insufficient ZnS shell formation shown in the TEM images. The PL-QY of the w/-heating NPs was drastically reduced by Zn doping. Several reports on the PL properties of Zn–Ag–In–S NPs and/or ZnS–$AgInS_2$ solid-solution NPs revealed that the PL-QY value depends on the Zn content.[12)-15)] Moreover, an optimum Zn content for PL enhancement exists, and excess Zn reduces PL intensity.[12),15)] Thus, the low PL-QY of the w/-heating NPs may be because of the high Zn content along with the nonradiative recombination centers created during ZnS capping.

To investigate the reason for this reduction in PL-QY values after capping with ZnS, the radiative and nonradiative recombination rates (k_{rad} and k_{nrad}, respectively) were evaluated. The total recombination rate of excited electrons and holes is given by the inverse of the PL decay time, τ_{PL}, by the following expression:[19)]

$$\frac{1}{\tau_{PL}} = k_{rad} + k_{nrad} \quad (1)$$

The PL-QY, η, is also calculated from the recombination rates:[19)]

$$\eta = \frac{k_{rad}}{k_{rad}+k_{nrad}} \quad (2)$$

Thus, we can calculate the values of k_{rad} and k_{nrad} using the above expressions when both η and τ_{PL} are known. The values of τ_{PL} of the original AIS, w/o-heating NPs, and w/-heating NPs were measured by excitation at 2.33 eV. Figure 5 shows the PL decay curves monitored at the PL peaks. There is no apparent difference between the decay behaviors of the original and w/o-heating NPs; however, the decay is faster in the w/-heating NPs. This result suggests that the recombination dynamics of the AIS cores of the w/o-heating NPs are equivalent to those in the original AIS NPs. The parameters k_{rad} and k_{nrad} evaluated from η and τ_{PL} are listed in Table 1. The k_{nrad} of the w/o-heating NPs is larger than that of the original AIS NPs, although their radiative recombination rates are almost the same. Consequently, the slightly lower PL-QY value of the w/o-heating NPs can be attributed to the relatively large amount of nonradiative recombination centers formed on the surfaces of the core AIS NPs during the shell formation process. A significant decrease in the k_{rad} and an increase in the k_{nrad} of the w/-heating NPs are observed; these effects may arise from the quaternary compositions of the NPs along with insufficient surface passivation.

We have shown that capping with ZnS shells did not passivate the nonradiative recombination centers on the surfaces of the AIS cores in the w/o-heating NPs; therefore,

the PL was not enhanced. To better understand the role of the ZnS shells, the NP structures were investigated in detail using PL excitation (PLE) spectroscopy. The PLE spectra of the original AIS and w/o-heating NPs (solid curves) are shown in Fig. 6 along with their absorption spectra (dashed curves). It has already been shown in Fig. 4 that the shape of the absorption spectrum of the w/o-heating NPs is identical to that of the spectrum of the original AIS NPs in the low-energy region, where only the AIS cores contribute to the absorption. In the region above ~4 eV, the absorption of the w/o-heating NPs abruptly increases, which is ascribed to the interband transition of the ZnS shells. In contrast, the PLE spectrum of the w/o-heating NPs is identical to both the PLE and absorption spectra of the original NPs, even above 4 eV. These results indicate that the excitation of the ZnS shells does not contribute to the PL of the AIS cores. If an identical core/shell structure with a type-I potential well structure, which is assumed to AIS/ZnS core/shell NPs, is constructed, wave functions of carriers excited to the energy levels above core/shell potential barriers spread over an entire NP including core and shell, whereas photo-excited carriers on the energy levels below potential barriers are localized in the core.[20] Therefore, in such identical core/shell NPs, excitation beyond the core/shell potential barrier (higher than ~4 eV in this case) produces PL of the cores much more effectively than in the original AIS NPs excited by the same energies. Consequently, these findings indicate that the electronic states of the AIS cores are isolated from those of the ZnS shells, implying that the interface between the AIS cores and the ZnS shells is poor in the w/o-heating NPs. These defective core/shell structures would have originated during the growth of ZnS shells at room temperature. The epitaxial growth of ZnS shells around CdSe NPs was observed in highly luminescent CdSe/ZnS core/shell NPs despite the large lattice mismatch between CdSe and ZnS (12%).[6] The lattice mismatch between AIS and ZnS is only 3–7 %. Therefore, annealing after ZnS shell formation at an appropriate temperature and duration may create high-quality core/shell interfaces without the penetration of Zn atoms into the AIS cores, possibly resulting in the significant enhancement of PL.

Acknowledgments

This work was partly supported by the Nanotechnology Platform Program (Molecule and Material Synthesis) of the Ministry of Education, Culture, Sports, Science and Technology (MEXT), Japan, and JSPS KAKENHI Grant Numbers 26400316 and 25420785. We would like to acknowledge Dr. T. Asaka for his assistance in the TEM observations. PLE spectra were collected at the Institute for Molecular Science, Okazaki, Japan.

References

1) H. Weller, Angew. Chem. Int. Ed. Engl. **32**, 41 (1993).
2) A. P. Alivisatos, J. Phys. Chem. **100**, 13226 (1996).
3) R. Rossetti and L. Brus, J. Phys. Chem. **86**, 4470 (1982).
4) A. I. Ekimov, A. L. Efros, and A. A. Onuschenko, Solid State Commun. **56**, 921 (1985).
5) M. A. Hines and P. Guyot-Sionnest, J. Phys. Chem. **100**, 468 (1996).
6) B. O. Dabbousi, J. Rodriguez-Viejo, F. V. Mikulec, J. R. Heine, H. Mattoussi, R. Ober, K. F. Jensen, and M. G. Bawendi, J. Phys. Chem. B **101**, 9463 (1997).
7) R. Xie, M. Rutherford, and X. Peng, J. Am. Chem. Soc. **131**, 5691 (2009).
8) J. Park and S. Kim, J. Mater. Chem. **21**, 3745 (2011).
9) H. Zhong, Z. Wang, E. Bovero, Z. Lu, F. C. J. M. van Veggel, and G. D. Scholes, J. Phys. Chem. C **115**, 12396 (2011).
10) L. Li, A. Pandey, D. J. Werder, B. P. Khanal, J. M. Pietryga, and V. I. Klimov, J. Am. Chem. Soc. **133**, 1176 (2011).
11) B. Mao, C. Chung, J. Wang and C. Burda, J. Phys. Chem. C **115**, 8945 (2011).
12) H. Nakamura, W. Kato, M. Uehara, K. Nose, T. Omata, S. Otsuka-Yao-Matsuo, M. Miyazaki, and H. Maeda, Chem. Mater. **18**, 3330 (2006).
13) W. Zhang and X. Zhong, Inorg. Chem. **50**, 4065 (2011).
14) X. Tang, W. B. A. Ho, and J. M. Xue, J. Phys. Chem. C **116**, 9769 (2012).
15) T. Torimoto, T. Kameyama, and S. Kuwabata, J. Phys. Chem. Lett. **5**, 336 (2014).
16) T. Ogawa, T. Kuzuya, Y. Hamanaka, and K. Sumiyama, J. Mater. Chem. **20**, 2226 (2010).
17) O. Madelung, *Semiconductors: Data Handbook*, (Springer-Verlag, Berlin, 2004).
18) N. Kumbhojkar, V. V. Nikesh, A. Kshirsager, and S. Mahamuni, J. Appl. Phys. **88**, 6260 (2000).
19) J. I. Pankove, *Optical Processes in Semiconductors*, (Dover Publications, New York, 1975) p. 112.
20) A. Mukherjee and S. Ghosh, J. Phys. D: Appl. Phys. **45**, 195103 (2012).

Figure Captions

Fig. 1. (a) HAADF-STEM images of the w/o-heating NPs. EDS elemental mapping images of the (b) Ag L-edge, (c) In L-edge, (d) Zn K-edge, and (e) S K-edge obtained from the same area. (f) An overlaid image.

Fig. 2. (a) HAADF-STEM images of the w/-heating NPs. EDS elemental mapping images of the (b) Ag L-edge, (c) In L-edge, (d) Zn K-edge, and (e) S K-edge obtained from the same area. (f) An overlaid image.

Fig. 3. (a) XRD patterns of the AIS, w/o-heating NPs, and w/-heating NPs collected using a powder diffractometer with CuKα radiation. (b) JCPDS data of tetragonal AIS. (c) JCPDS data of cubic ZnS.

Fig. 4. Absorption and PL spectra of AIS (black), w/o-heating (blue), and w/-heating (red) NPs. Absorption spectra are plotted on a logarithmic scale for clarity.

Fig. 5. PL decay curves of AIS (black), w/o-heating (blue), and w/-heating (red) NPs. Dotted lines indicate the results of fitting analyses.

Fig. 6. PLE spectra of AIS NPs (black solid line) and w/o-heating NPs (blue solid line). The inset is an enlarged view of the PLE spectra. The absorption spectra of AIS NPs (black dashed line) and w/o-heating NPs (blue dashed line) are also shown.

Table I. Photoluminescence parameters of NPs.

sample	η	τ_{PL} (μs)	k_{rad} (s^{-1})	k_{nrad} (s^{-1})
original AIS	0.242 ± 0.014	0.56	$(4.3 \pm 0.2)\times10^5$	$(13.5 \pm 0.3)\times10^5$
w/o-heating	0.191 ± 0.009	0.50	$(3.8 \pm 0.2)\times10^5$	$(16.3 \pm 0.2)\times10^5$
w/-heating	0.081 ± 0.004	0.38	$(2.1 \pm 0.1)\times10^5$	$(24.0 \pm 0.1)\times10^5$

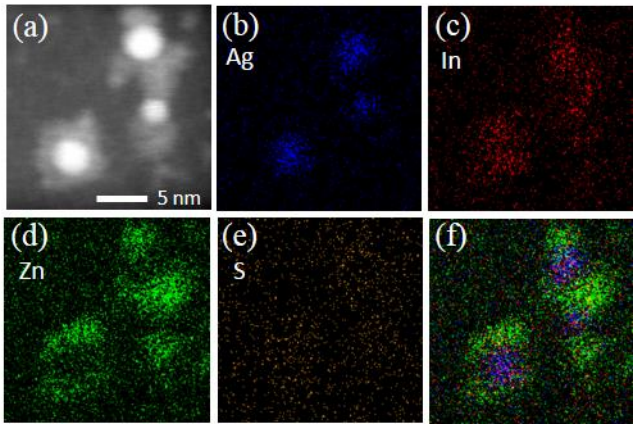

Fig. 1. Y. Hamanaka et al.

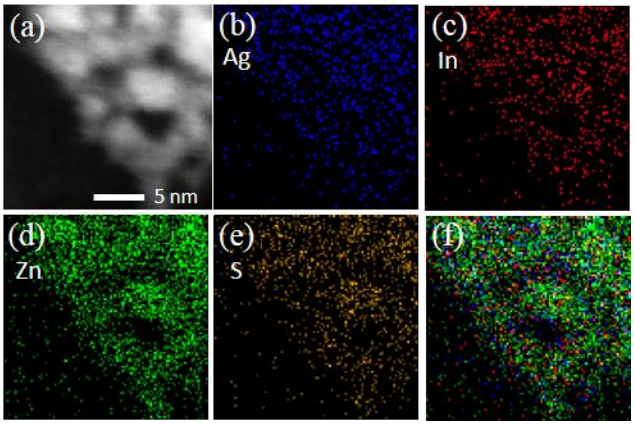

Fig. 2. Y. Hamanaka et al.

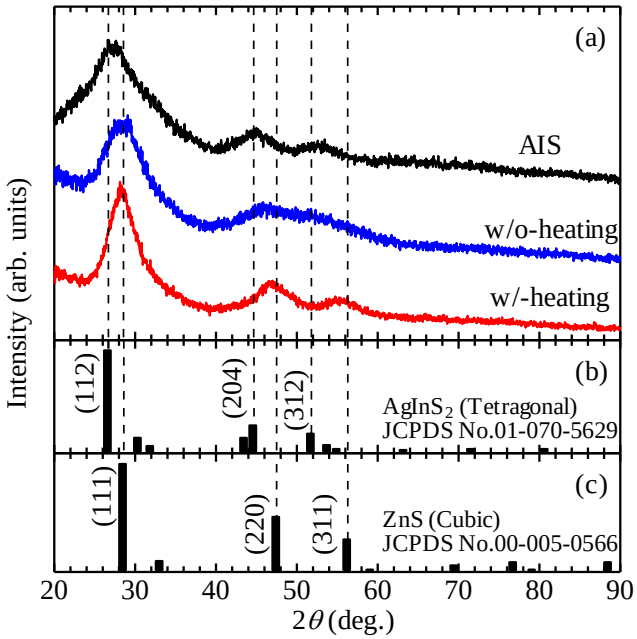

Fig. 3. Y. Hamanaka et al.

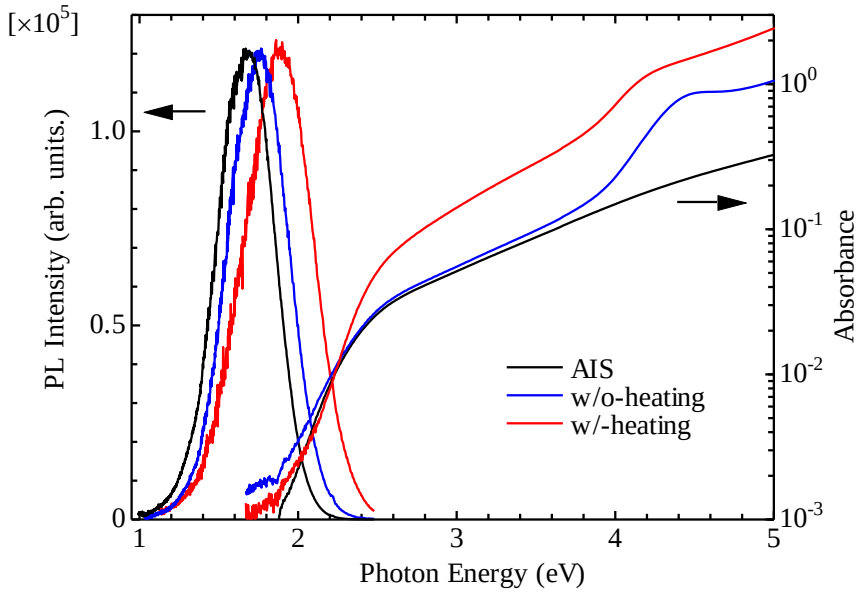

Fig. 4. Y. Hamanaka et al.

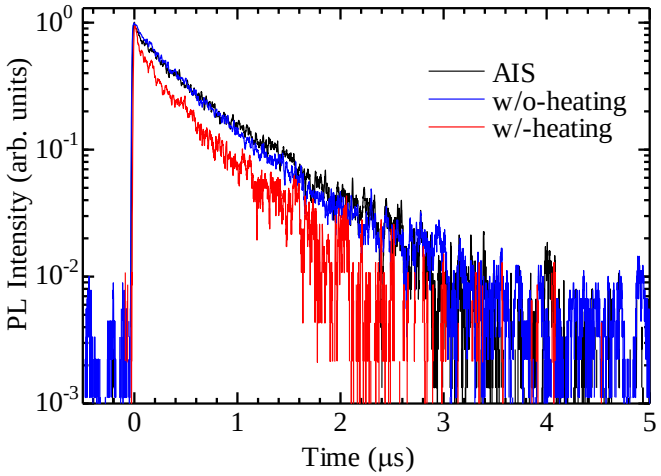

Fig. 5. Y. Hamanaka et al.

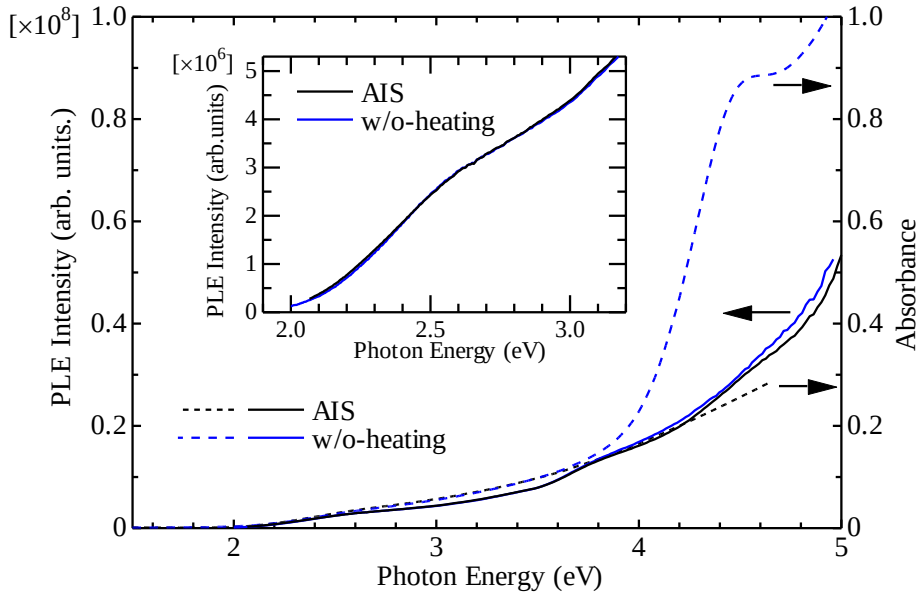

Fig. 6. Y. Hamanaka et al.